

# CHARACTERIZING THE MICROSTRUCTURAL AND MICROMECHANICAL PROPERTIES OF SNOW

Jerome B. Johnson<sup>\*</sup>  
U.S. Army Cold Regions Research and Engineering Laboratory

Martin Schneebeli  
Swiss Federal Institute for Snow and Avalanche Research

**ABSTRACT:** A micropenetrometer has been developed that produces snow grain bond ruptures at the microstructural level and provides a unique signal for different snow types (Johnson and Schneebeli, 1997; Schneebeli and Johnson, 1998). A micromechanical theory of penetration has been developed and used to recover microstructural and micromechanical parameters for different snow types from the penetration force-distance signal. These parameters are the microstructural element dimension, the mean grain size, the critical microstructural deflection at rupture and the microstructural coefficient of elastic restitution. Additional derived mechanical properties include the compression strength and elastic modulus of microstructural elements and continuum scale volumes of snow. Analysis of the force-distance signal from a Monte Carlo simulation of micropenetration indicates that microstructural and micromechanical parameters may be recovered with an accuracy of better than 5% when spatial and force resolutions are high and the penetrometer tip area is of similar size to the structure dimension.

**KEYWORDS:** snow hardness, snow engineering, snow strength, snow mechanics

## 1. INTRODUCTION

The mechanical properties of snow depend on its internal microstructure, density, temperature, wetness and rate of loading (or deformation). Of these factors, no satisfactory way of determining snow microstructure and its influence on snow deformation has been found, despite much effort. The problem is difficult as the microstructure consists of snow grain size and shape, intergrain bond size, shape and number, and the larger scale geometry of chains of connected grains. An added difficulty is to determine how the microstructure affects snow mechanical properties.

Because of the difficulties of determining snow microstructure and relating it to mechanical properties, efforts to characterize snow through field measurements have focused primarily on large diameter cone index measurements (diameters much larger than the structural element size). The rammsonde is the most widely used and accepted large diameter penetrometer and has the advantage of being relatively simple and rapid to use. It may also be correlated with snow strength, in a general way, and can delineate layering in the

snow cover, which is of interest for avalanche hazard evaluation. Unfortunately, the rammsonde and other traditional large diameter cone penetrometers have several draw backs that severely limit their usefulness. Their large diameter and cone length prevent them from detecting the thin layers often responsible for the formation of avalanches (Bader et al., 1954). In addition, correlations between cone index and snow mechanical strength generally show a large degree of scatter (Abele, 1990).

To improve the ability to detect thin layers in snow and to determine snow mechanical properties Martin Schneebeli and I developed a small diameter cone penetrometer (Johnson and Schneebeli, 1997; Schneebeli and Johnson, 1998). These efforts demonstrated that micropenetrometer force measurements are caused by the rupturing of microstructural elements in the snow. Two different methods for interpreting the penetration force-distance records are under active investigation. The first method uses a statistical correlation between force measurements and defined structural factors (Pielmeier, 1998; Schneebeli et al., this issue).

---

<sup>\*</sup> *Corresponding author address:* Jerome B. Johnson, U.S. Army Cold Regions Research and Engineering Laboratory, P.O. Box 35170, Ft. Wainwright, AK 99703-0170, email: jjohnson@crrel.usace.army.mil

The second method, presented in this paper, is based on the micromechanical processes associated with cone penetration and has the advantage of directly interpreting the micropenetrator force-distance record in physical terms.

## 2. MODEL OF PENETRATION

The purpose of constructing a micromechanical model of penetration for a small dimension penetrator is to develop a way to characterize snow microstructure by its mechanical behavior. Once this is done, different snow types may be classified by their mechanical behavior and morphological features. Such classification is necessary to solve engineering problems in snow covered regions and to better assess snow slab stability.

The assumptions required for the micromechanical penetration model are:

- The penetrator force-displacement record is caused by penetrator/ice friction, and the elastic deflection and rupture of microstructural elements.
- The effects of material compaction are negligible (this assumption is not completely correct, but results in minimal errors for very porous materials).
- The microstructural elements have a mean constant dimension,  $L_n$ , but are randomly distributed.

The penetration force acting along the axis of penetration is given by

$$F_p = N_a f_p \quad (1)$$

where  $N_a$  is the number of intact structural elements in contact with the penetrator face,  $f_p$  is the axial force contribution of each microstructural element (Fig. 1).

The number of microstructural elements in contact with a penetrator is determined by the number of available intact elements in front of the penetrator face and the probability of their contact. The number of available intact microstructural elements is given by

$$N_s = \frac{A_s}{L_n^2} \quad (2)$$

where  $A_s$  is the surface area of the penetrator and  $L_n$  is the mean dimension of microstructural elements normal to the penetrator face. The probability of contact can be estimated as

$$P_c = \frac{\delta_{n,r}}{L_n} \quad (3)$$

where  $\delta_{n,r}$  is the elastic deflection of the microstructural element normal to the penetrator face at the point of rupture (Gibson and Ashby, 1988).

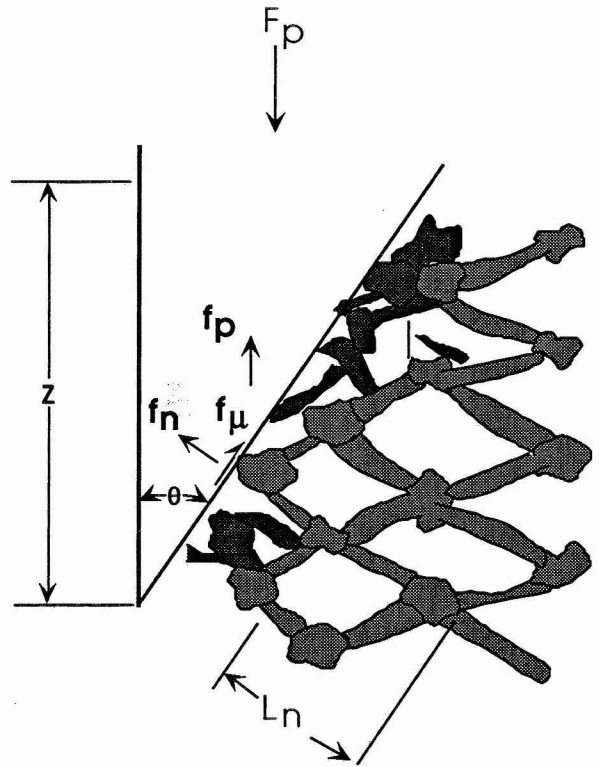


Fig. 1. Cone penetrator interaction with microstructural snow elements.

Over the area  $A_s$ , the number of intact elements in active contact with the penetrator can be described using a binomial distribution with mean

$$\bar{N}_a = N_s P_c \quad (4)$$

and variance about the mean

$$\sigma_{N_c}^2 = N_s P_c (1 - P_c) \quad (5)$$

Consequently, the number of microstructural units in active contact at any position is given by

$$N_a = N_s P_c \pm M_c \sqrt{N_s P_c (1 - P_c)} \quad (6)$$

(Gibson and Ashby, 1988). The parameter  $M_c$  is a multiplier that determines the number of standard deviations about the mean that contribute. Experiments on foams indicate the maximum value of  $M_c$  is about 3. The physical interpretation of  $M_c$  can be understood from a statistical view by recognizing that the binomial distribution can approach the Gaussian form for large  $N_s$ . For a Gaussian distribution, 0.999% of all events are included within three standard deviations of its mean. Hence, for all practical purposes  $M_c = 3$  includes all possible events and yields the maximum number of active contacts

$$N_{a,max} = N_s P_c \pm 3 \sqrt{N_s P_c (1 - P_c)} \quad (7)$$

While comparison of the binomial and Gaussian distributions is statistically valid only for large  $N_s$ , experiments on zirconia foam indicate that the statistical maximum at  $M_c = 3$  may also yield reasonable results for small  $N_s$  (Gibson and Ashby, 1988).

The force exerted by a single microstructural element in contact with a penetrometer is the result of elastic deflection of the element and friction between the ice and penetrometer and is given by

$$f_p = (f_n \sin \theta + f_\mu \cos \theta) = f_n (1 + \mu \cot \theta) \sin \theta \quad (8)$$

where  $f_n$  is the normal force acting on the penetrometer face due to elastic deflection of individual microstructural elements,  $f_\mu$  is the tangential frictional force between the snow and penetrometer face,  $\mu$  is the friction coefficient and  $\theta$  is the half angle between the axis of penetration and the penetrometer face (Fig. 1). The normal and frictional forces are given by

$$f_n = k_n \delta_n \quad (9)$$

$$f_\mu = \mu f_n$$

where  $k_n$  is the elastic coefficient of restitution and  $\delta_n$  is the elastic deflection of a microstructural element.

The total force acting on the penetrometer is the sum of the forces of all structural elements in contact (i.e., the product of the number of contacts and the mean force exerted by each element). Two possible conditions of microstructural element force state are of interest. The first condition consists of a penetrometer in contact with a complementary snow surface shape (e.g., a flat penetrometer/indenter and a flat snow surface) prior to microstructural element rupture. Here, the force exerted by each of the active contacts on the penetrometer is the same and is given by Eq. 8. The total force of penetration before rupturing begins is given by Eq. 1 and the maximum force (or first peak failure force) is given by

$$F_{p,peak} = N_{a,max} f_{p,r} \quad (10)$$

where  $f_{p,r}$  is the force of rupture for a microstructural element and is given by

$$f_{p,r} = f_{n,r} (1 + \mu \cot \theta) \sin \theta \quad (11)$$

and

$$f_{n,r} = k_n \delta_{n,r} \quad (12)$$

where  $\delta_{n,r}$  is the microstructural element deflection at rupture.

The second force condition of interest occurs after the initial rupture of microstructural elements that produces a randomly distributed surface geometry of intact microstructural elements. In this situation, the deflection and force exerted on a penetrometer by any microstructural element in contact has an equal probability of taking any value between zero and  $f_{p,r}$ . This condition is described by a uniform probability distribution with probability density function

$$P(f_{p,r}) = \begin{cases} \frac{1}{f_{p,r}} & 0 < f_p \leq f_{p,r} \\ 0 & elsewhere \end{cases} \quad (13)$$

with mean

$$\bar{f}_{p,r} = \frac{f_{p,r}}{2} \quad (14)$$

and variance

$$\sigma_{\bar{f}_{p,r}}^2 = \frac{1}{3} \left( \frac{f_{p,r}}{2} \right)^2 \quad (15)$$

The possible range of forces exerted by each microstructural element is, from Eqs. 14 and 15,

$$f_p = \bar{f}_{p,r} \left( 1 \pm M_f \sqrt{\frac{1}{3}} \right) \quad (16)$$

where  $M_f$  is the multiplier that determines the number of standard deviations about the mean to include. The maximum force is given when  $M_f = \sqrt{3}$  which yields the force of rupture, as expected.

The total penetration force is given by Eq. 1 and is found by combining Eqs. 4, 5, 14 and 15 along with the standard deviation.

$$F_p = \bar{N}_a \bar{f}_{p,r} \pm \sqrt{\bar{f}_{p,r}^2 M_c^2 \sigma_{\bar{N}_a}^2 + \bar{N}_a^2 M_f^2 \sigma_{\bar{f}_{p,r}}^2} \quad (17)$$

and when substitutions are made for the average and variance values in the standard deviation

$$F_p = N_s P_c \frac{f_{p,r}}{2} \pm \left[ \left( \frac{f_{p,r}}{2} \right)^2 M_c^2 N_s P_c (1 - P_c) + (N_s P_c)^2 \frac{M_f^2}{3} \left( \frac{f_{p,r}}{2} \right)^2 \right]^{1/2} \quad (18)$$

When the multipliers are set to their maximum values and the penetrometer area is much greater than  $L_n^2$  then Eq. 18 becomes equivalent to the first peak force, Eq. 10.

### 3. MODEL VERIFICATION

Verification of the micromechanical penetration model was done by comparing calculated model results with the measured penetration stress for zirconia foam and with the results of a Monte Carlo simulation of penetration. Ashby et al. (1986) conducted a series of penetration tests in zirconia foam using a flat faced penetrometer/indenter. In these tests, the initial penetration stress increased to a peak then fell back to near zero. Continued penetration produced wild fluctuations with secondary peaks about half of the first maximum peak (First Peak).

The results of Ashby et al. (1986) are shown in Fig. 2 along with the calculated penetration stress from the micromechanical model. The values for micromechanical deflection at rupture and mean microstructural dimension were taken from Gibson and Ashby (1988) and the value for the coefficient of elastic restitution was set by fitting to the data. The penetration/indenter stress (also called penetration resistance) was calculated using

$$R_{p,peak} = \frac{F_{p,peak}}{A_b} = k_n \delta_{n,r} \frac{A_s}{A_b L_n^2} \frac{\delta_{n,r}}{L_n} \left( 1 - \frac{\delta_{n,r}}{L_n} \right) + 3 \sqrt{\frac{L_n^2}{A_s} \frac{L_n}{\delta_{n,r}} \left( 1 - \frac{\delta_{n,r}}{L_n} \right)} \quad (19)$$

for the First Peak penetration stress and

$$R_{p,max} = \frac{F_{p,max}}{A_b} = \frac{k_n \delta_{n,r}}{2} \frac{A_s}{A_b L_n^2} \frac{\delta_{n,r}}{L_n} \left( 1 - \frac{\delta_{n,r}}{L_n} \right) + 3 \sqrt{\frac{L_n^2}{A_s} \frac{L_n}{\delta_{n,r}} \left( 1 - \frac{\delta_{n,r}}{L_n} \right)} \quad (20)$$

for the Maximum continuous penetration stress.

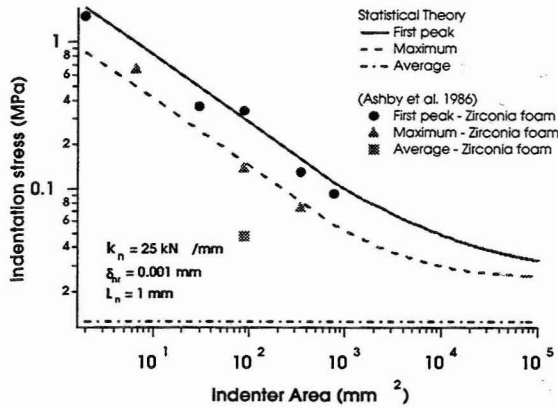


Fig. 2 Comparison of micromechanical theory with First Peak and Maximum penetration/indentation stress for zirconia foam, data from Ashby et al. (1986).

For a flat faced penetrometer,  $A_b = A_s$  so that the mean penetration stress is independent of penetrometer base area. However, the standard deviation contribution to the stress decreases as  $\sqrt{1/A_s}$  causing the penetration/indentation stress to decrease as  $\sqrt{1/A_s}$  until the ratio of penetrometer surface area to structure area becomes very large.

The agreement between theory and experiment is very good for First Peak and Maximum. Where First Peak is defined as the maximum penetration stress that occurs prior to rupture initiation and Maximum is the maximum penetration stress that occurs during continuous penetration after the initial rupture. The average calculated penetration stress is, however, much lower than the measured data and better represents the minimum stresses. This is a consequence of not including the effects of compaction in the model. As a material compacts the broken fragments from microstructural element rupture pack together, increasing the probability of contact and the average penetration stress. It is apparent, however, that First Peak and Maximum penetration stresses for the zirconia are not significantly affected by compaction.

The results of a Monte Carlo simulation of penetration in a hypothetical cohesive-elastic-brittle granular material are shown in Fig. 3. In the top panel the force- penetration distance record is shown for a single column of microstructural elements.

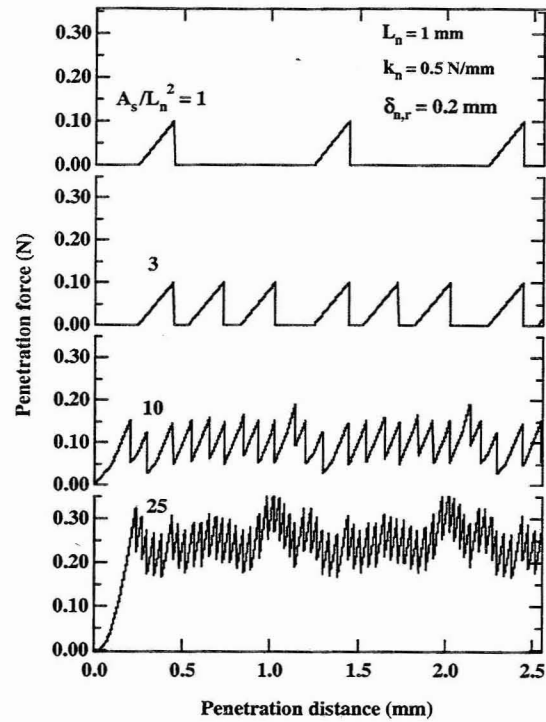


Fig. 3. Monte Carlo simulation of penetration

When the penetrometer contacts a microstructural element the force increases until the element ruptures then the force immediately drops to zero. The force remains at zero until contact with the next intact microstructural element is made. The mean separation of microstructural elements in any column is constant. The position of the starting point of adjacent columns of microstructural elements can, however, be at any position between 0 and  $L_n$ .

In the bottom three panels of Fig. 3 the force-penetration distance records for 3, 10 and 25 columns with randomly selected starting positions between 0 and  $L_n$  are shown. These correspond to penetrometers with progressively larger surface areas moving continuously through the material. The results are remarkably similar to those obtained from micropenetrometer tests in snow (Fig. 4).

The statistics from the Monte Carlo simulation and the microstructural penetration model are shown in Table 1.

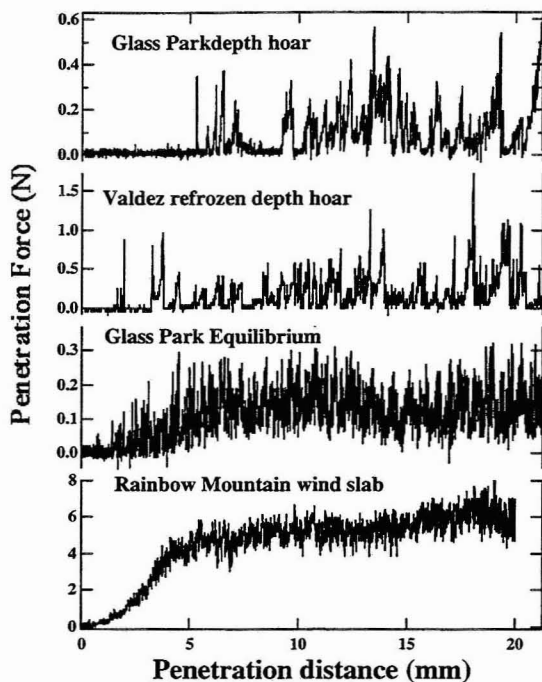


Fig. 4. Micropenetrometer force-distance record for four different Alaskan snow types (Johnson et al., 1997).

The agreement between the force statistics is quite good. The agreement of the mean penetration force magnitudes is the most important indication that the micromechanical model is yielding reasonable results. This is because the mean penetration force is the same irrespective of how the spacing between contacts occurs. The maximum penetration force, however, is strongly dependent on the variation of the force about the mean and varies with contact spacing. For example, when  $A_g/L_n^2 = 3$  the mean force is 0.03 N no matter how the contacts are spaced. If the contact spacing is such that only one contact occurs at a time then the maximum penetration force is 0.1 N. If however all of the contacts occur at the same time, as happens during first peak rupture, the maximum penetration force would be 0.3 N. Consequently, a random distribution produces maximum penetration forces somewhere between the average and first peak penetration force magnitudes. A comparison of Monte Carlo and micromechanical First Peak force magnitudes is not presented as it is obvious that they would agree.

	$A_g/L_n^2$	$F_{p,max}$ (N)	$F_{p,mean}$ (N)
micromechanical Monte Carlo	1	0.07 0.12	0.01 0.01
micromechanical Monte Carlo	3	0.13 0.1	0.03 0.03
micromechanical Monte Carlo	10	0.29 0.19	0.1 0.095
micromechanical Monte Carlo	25	0.55 0.37	0.25 0.23

Table 1. Comparison of penetration force statistics between Monte Carlo simulation and micromechanical model.

#### 4. DERIVATION OF MICROSTRUCTURAL AND MICROMECHANICAL PARAMETERS

The micromechanical model can predict the penetration force-distance response when the microstructural ( $L_n$ ) and micromechanical ( $k_n$  and  $\delta_{n,r}$ ) properties of a granular material are well characterized. Conversely, with good quality penetration force-distance data, it should be possible to use the micromechanical model to recover microstructural and micromechanical properties and use them to characterize the material.

Before using the micromechanical model to interpret micropenetrometer data we must make two additional assumptions:

- e. Any microstructural element in contact with the penetrometer will rupture within a penetration travel distance of  $L_n$ .
- f. Micropenetration force spikes are caused by the rupture of individual microstructural elements.

Assumption (e) allows the reasonable association between the number of failure peaks detected in a given penetration travel distance with the mean structural dimension  $L_n$ . The number of microstructural elements that fail during a penetration travel distance  $z_p$  is a function of the surface area of the penetrometer and the spacing between microstructural elements and can be expressed as

$$n_{peaks} = \frac{z_p A_g}{L_n L_n} \quad (21)$$

Rearranging Eq. 21 to find  $L_n$  yields

$$L_n = \left( \frac{z_p}{n_{peaks}} A_s \right)^{1/3} \quad (22)$$

The consequence of assumption (f) is that each drop in penetration force seen in the penetration force-distance data is interpreted as a direct measure of the rupture force  $f_{p,r}$ . Using the definition of mean penetration force

$$\bar{F}_p = \frac{f_{p,r} A_s}{2 L_n^2} P_c \quad (23)$$

and the fact that  $\bar{F}_p$  and  $f_{p,r}$  can be determined from micropenetrometer data provides a way to calculate the probability of contact

$$P_c = \frac{2 L_n^2 \bar{F}_p}{f_{p,r} A_s} \quad (24)$$

The definition of  $P_c$  given in Eq. 3 and Eq. 24 can be combined to find the microstructural deflection at rupture

$$\delta_{n,r} = \frac{2 L_n^3 \bar{F}_p}{f_{p,r} A_s} \quad (25)$$

The microstructural rupture force normal to the penetrometer face is found by inverting Eq. 11 giving

$$f_{n,r} = \frac{f_{p,r}}{(1+\mu \cot \theta) \sin \theta} \quad (26)$$

and Eqs. 12 and 26 are used to calculate the coefficient of elastic restitution

$$k_n = \frac{f_{p,r}}{\delta_{n,r} (1+\mu \cot \theta) \sin \theta} \quad (27)$$

One additional microstructural parameter, the grain size, can be defined using the microstereological definition of relative density from point counting methods

$$L_s = L_n \frac{\rho_0}{\rho_s} \quad (28)$$

where  $L_s$  is the calculated grain dimension,  $\rho_0$  is the initial material density and  $\rho_s$  is the solid material density.  $L_s$  does not have the same interpretation as in microstereology as it is not derived from relative volume considerations, but is, instead, a result of the distance between microstructural elements as determined by their contact with the penetrometer. As a consequence,  $L_s$  is probably a function of both grain shape and size.

For engineering interpretation of snow mechanical properties, the properties  $L_n$ ,  $\delta_{n,r}$  and  $k_n$  are not easily understood. However, they can be used to derive the more commonly used properties of compaction strength and elastic modulus for both micromechanical and macromechanical scales. The micromechanical compaction strength and elastic modulus for a microstructural element are given by

$$\sigma_n = \frac{f_{n,r}}{L_n^2} \quad (29)$$

and

$$E_n = \frac{k_n}{L_n} \quad (30)$$

respectively. The corresponding macromechanical compaction stress and elastic modulus are controlled by the number of active contacts and are given by

$$\sigma_{macro} = \sigma_n P_c = \frac{f_{n,r} \delta_n}{L_n^2 L_n} \quad (31)$$

and

$$E_{macro} = E_n P_c = E_n \frac{\delta_n}{L_n} \quad (32)$$

In Table 2, the microstructural parameter  $L_n$  and micromechanical parameters  $\delta_{n,r}$  and  $k_n$  calculated using Eqs. 22, 25 and 27 from the Monte Carlo simulation results are compared with the corresponding input parameters to the simulation. The agreement is quite good. For  $A/L_n^2 = 1$  and 3 there is no difference between the

calculated and actual parameter values. The difference between calculated values and actual is about 5% for  $A/L_n^2 = 10$  and about 10% for  $A/L_n^2 = 25$ . These results indicate that it may be possible to recover the microstructural and micromechanical parameters for snow to quite high accuracy, especially with low  $A/L_n^2$  ratios.

	$A_s$ (mm <sup>2</sup> )	$L_n$ (mm)	$\delta_{n,r}$ (mm)	$k_n$ (N/mm)
Calculated	1	1	0.2	0.5
Calculated	3	1	0.2	0.5
Calculated	10	1	0.19	0.526
Calculated	25	1	0.18	0.556
Actual		1	0.2	0.5

Table 2. Comparison of microstructural and micromechanical properties calculated from Monte Carlo data using Eqs. 22, 25 and 27.

## 5. CHARACTERIZATION OF SNOW MICROSTRUCTURE AND MICROMECHANICAL PROPERTIES

Johnson et al. (1997) collected four different snow types in Alaska and conducted snow micropenetrometer measurements on them. The snow samples consisted of hard wind slab, a low density equilibrium metamorphosed snow, a depth hoar sample and a depth hoar sample that had thawed and then been refrozen. The force-penetration distance record for each sample was analyzed using the micromechanical penetration theory to characterize snow types by their microstructural and micromechanical properties. In Table 3, the measured density, sieve grain size and microstructural and micromechanical properties derived from the force-penetration records are given. The microscale and macroscale compression strength and elastic moduli for the four snow types are given in Table 4. Several interesting features in the microstructural and micromechanical parameters are readily apparent and agree with field observations of snow characteristics. The microstructural element dimension,  $L_n$ , is significantly larger for the two depth hoar samples (GPDH and VDH) than for the equilibrium and wind slab samples (GPEQ and RMWS).

	GPEQ	GPDH	VDH	RMWS
Density (kg/m <sup>3</sup> )	229	238	280	400
Sieve grain size (mm)	0.6	1.2	1.2	0.4
$L_n$ (mm)	1.65	3.62	3.58	1.45
$f_{n,r}$ (N)	0.32	0.48	1.6	3.8
$k_n$ (N/mm)	2	1.26	4.71	31.67
$\delta_{n,r}$ (mea) (mm)	0.16	0.38	0.34	0.12
$\delta_{n,r}$ (cal) (mm)	0.1	0.34	0.2	0.34
$L_s$ (mm)	0.41	0.94	1.09	0.63

Table 3. Microstructural and micromechanical parameters for Glass Park Equilibrium (GPEQ), Glass Park depth hoar (GPDH), Valdez refrozen depth hoar (VDH) and Rainbow Mountain wind slab (RMWS). Data are from Alaskan snow types (Johnson et al., 1997).

The equilibrium and wind slab microstructural element dimensions are similar to each other. The force of rupture for the snow samples increases along with snow density, but not linearly. The equilibrium snow has a very low rupture strength. While the density change from lowest to highest was slightly less than a factor of two, the range of rupture force, from lowest to highest, was about a factor of 10. Examination of the coefficient of elastic restitution,  $k_n$ , indicates that the wind slab (RMWS) was the stiffest (highest  $k_n$ ) and most brittle snow type (lowest  $\delta_{n,r}$ ). Finally, the shape dependent grain size parameter,  $L_s$ , varied in the same fashion as the sieve grain size. Equilibrium and wind slab show the smallest grain sizes and the two depth hoars the largest. The shape factor influence on  $L_s$  may be observed by noting that the two depth hoar  $L_s$  values are about equal, as are their sieve grain sizes. The equilibrium snow, however, has an  $L_s$  value that is significantly less

that the wind slab value, just the reverse of their sieve grain size comparison where the wind slab sieve grain size is smaller than for the equilibrium snow. This reversal between  $L_s$  and the sieve grains is interpreted as being due to differences in grain shape. The measured deflection at rupture,  $\delta_{n,r}$  (mea), and deflection at rupture calculated from Eq. 25,  $\delta_{n,r}$  (cal), are given in table 3. It is apparent that the calculated deflection can differ from measured values significantly, especially for the wind slab sample. We interpret this to be the result of compaction effects that are not included in the theory.

Comparison of microscale and macroscale compressive strength and elastic modulus demonstrate the complexity of snow structural influences on snow mechanical properties. At the microscale the equilibrium snow (GPEQ) has comparable compressive strength and elastic modulus as Valdez refrozen depth hoar even though its density is less (Table 4). The Glass Park depth hoar has the lowest microscale compression strength and elastic modulus and the wind slab the highest, as expected. The magnitudes of compressive strength and elastic modulus for all four snow types is much lower at macroscales than microscales. This occurs because the microscale properties describe the characteristics of a single microstructural element.

	GPEQ	GPDH	VDH	RMWS
$\sigma_n$ (MPa)	0.12	0.04	0.13	1.79
$E_n$ (MPa)	1.21	0.35	1.31	21.76
$\sigma_{macro}$ (MPa)	0.011	0.004	0.012	0.15
$E_{macro}$ (MPa)	0.12	0.04	0.13	1.79

Table 4. Microstructural element compressive strength,  $\sigma_n$ , and elastic modulus,  $E_n$ , and macroscale compressive strength,  $\sigma_{macro}$ , and elastic modulus,  $E_{macro}$  for Glass Park Equilibrium (GPEQ), Glass Park depth hoar (GPDH), Valdez refrozen depth hoar (VDH) and Rainbow Mountain wind slab (RMWS). Data are from Alaskan snow types (Johnson et al., 1997).

The macroscale properties are, however, affected strongly by the number of microstructural elements that may contact available to support a load and this is determined by the probability of contact. The probability of contact decreases with sample size resulting in a corresponding decrease in compressive strength and elastic modulus magnitudes.

The manner in which the probability of contact is defined produces the coincidence that the macroscale elastic modulus is identical to the microscale compressive strength. This occurs because of the way the probability of contact is defined (Eq. 3). The probability of contact is equivalent to the microstructural element strain at rupture. This is a reasonable result for highly porous snow, but may be less reasonable when compaction effects or high densities (densities near critical) may result in probabilities of contact that are much higher than Eq. 3 predicts.

## 5. CONCLUSIONS

A statistically based micromechanical theory of cone and flat surface penetration into snow has been developed. Microstructural and micromechanical parameters have been derived from the theory to characterize different snow types. The strong agreement between the model for penetration and Monte Carlo simulation results support the observation that snow structure is a critical controlling factor in snow mechanical behavior. High resolution force-distance penetration measurements interpreted using the micromechanical model provide accurate, quantitative microstructural and micromechanical property data for snow. This data can be used to estimate microscale and macroscale compression strength and elastic modulus properties.

## REFERENCES

- Abele, G. 1990: Snow roads and runways. USA Cold Regions Research and Engineering Laboratory, Monograph No. 90-3.
- Ashby, M.F., Palmer, A.C., Thouless, M., Goodman, D.J., Howard, M., Hallam, S.D., Murrell, S.A.F., Jones, H, Sanderson, T.J.O. and A.R.S. Pointer, 1986: Nonsimultaneous failure and ice loads on Arctic structures. In: 18 th Annual

Offshore Technology Conference, Houston, TX  
USA OTC, 399-404.

Bader, H., Haefeli, R., Bucher, E., Neher, J., Eckel,  
O. and Thams. C., 1954: Snow and its  
metamorphism. *Snow Ice and Permafrost  
Research Establishment, Translation No. 14.*

Gibson, L.J. and Ashby, M.F., 1988: Cellular  
solids, structures and properties. *Oxford; New  
York: Pergamon Press.*

Johnson, J.B. and Schneebeli, M., 1997: *US  
Patent Application 08/850,160.*

Johnson, J.B., Schneebeli, M., Barrett, S., Sturm,  
M. and Holmgren, J., 1997: Unpublished snow  
micropenetrometer test data on four different  
Alaskan snow types.

Schneebeli, M. and Johnson, J.B.: 1998: *Ann.  
Glaciol.*, **26**, 107-111.

Schneebeli, M., Pielmeier, C. and Johnson, J.B:  
1998. Measuring snow structure and hardness  
using a high resolution penetrometer of snow (this  
issue).